PAPER

Dielectric constant of flagellin proteins measured by scanning dielectric microscopy†

Helena Lozano,‡[a] Rene Fabregas, ‡[a] Núria Blanco-Cabra,[b] Rubén Millán-Solsona,[a,c] Eduard Torrents,[b] Laura Fumagalli[d,e] and Gabriel Gomila *[a,c]

The dielectric constant of flagellin proteins in flagellar bacterial filaments ~10–20 nm in diameter is measured using scanning dielectric microscopy. We obtained for two different bacterial species (*Shewanella oneidensis* MR-1 and *Pseudomonas aeruginosa* PAO1) similar relative dielectric constant values ε_{So} = 4.3 ± 0.6 and ε_{Pa} = 4.5 ± 0.7, respectively, despite their different structure and amino acid sequence. The present results show the applicability of scanning dielectric microscopy to nanoscale filamentous protein complexes and to general 3D macromolecular protein geometries, thus opening new avenues to study the relationship between the dielectric response and protein structure and function.

Received 1st August 2018,
Accepted 15th September 2018

Introduction

The electric polarizability of proteins, represented in mean field theories by the relative dielectric constant,[1,2] has long been recognized as a key parameter in determining the protein structure and their electrostatic interactions with charged biomolecules and ligands.[3–6] The dielectric constant determines the degree by which electric fields are screened by the protein microscopic electric dipoles themselves. As such, it has a strong effect on charge–charge and charge–dipole interactions in, and between, proteins, and hence, on the electrostatic energy contribution to protein folding, protein–protein, protein–DNA and protein–charged ligand interactions.[7]

Recently, we have developed a technique that we refer to here as scanning dielectric microscopy able to access directly the dielectric constant of small scale macromolecular biological systems.[8,9] The method has already enabled determining the dielectric constant of proteins in empty virus capsids and in virus tails[8,9] as well as of proteins in sub-micrometric protein mono-layer patches.[10] In all cases, the obtained protein relative dielectric constants under dry air conditions were $\varepsilon_r \sim 3$–4, in good agreement with the values reported from bulk measurements on dry protein powders, $\varepsilon_r \sim 2$–5[11,12] and with theoretical predictions excluding charged side chains, $\varepsilon_r \sim 4$.[4]

In the present work, we extend the applicability of scanning dielectric microscopy to measure the dielectric constant of macromolecular protein complexes forming sub-10 nm diameter nanoscale filamentous structures (and in general, to any sub-10 nm size 3D geometry). The present study, by dealing with low polarizable sub-10 nm nanofilaments, goes well beyond earlier studies on the conducting (rather than dielectric) properties of organic and inorganic nanofilament structures, such as DNA,[13] carbon nanotubes,[13–15] or semiconductor nanowires.[16] Filamentous macromolecular protein complexes include important protein systems like actin or myosin filaments, microtubules, intermediate filaments, amyloid fibers or bacterial polar flagella, which is the specific case considered in the present work. These systems are fundamental in the biology of cells and, in some cases, play a central role in important diseases.[17]

Results and discussion

We measured the dielectric constant of the flagellin proteins in bacterial polar flagella of two different bacterial species, namely, *Shewanella oneidensis* MR-1 and *Pseudomonas aerugi-*

[a]*Nanoscale Bioelectrical Characterization, Institute for Bioengineering of Catalonia (IBEC), The Barcelona Institute of Science and Technology (BIST), c/ Baldiri i Reixac 11-15, 08028 Barcelona, Spain. E-mail: ggomila@ibecbarcelona.eu*

[b]*Bacterial Infections: Antimicrobial Therapies, Institute for Bioengineering of Catalonia (IBEC), The Barcelona Institute of Science and Technology (BIST), c/ Baldiri i Reixac 11-15, 08028 Barcelona, Spain*

[c]*Departament d'Enginyeria Electrònica i Biomèdica, Universitat de Barcelona, C/ Martí i Franqués 1, 08028 Barcelona, Spain*

[d]*School of Physics and Astronomy, University of Manchester, Manchester M13 9PL, UK*

[e]*National Graphene Institute, University of Manchester, Manchester M13 9PL, UK*

†Electronic supplementary information (ESI) available: Additional information is provided on tip deconvolution, tip calibration and tip–sample distance, dependence of the capacitance gradient on flagellum length, tip radius, relative dielectric constant, flagellum curvature, dielectric constant extraction from dielectric approach curves and validation with full EFM dielectric profiles, parameters for the different flagella analyzed, and numerical calculations. See DOI: 10.1039/c8nr06190d

‡Equally contributing authors.

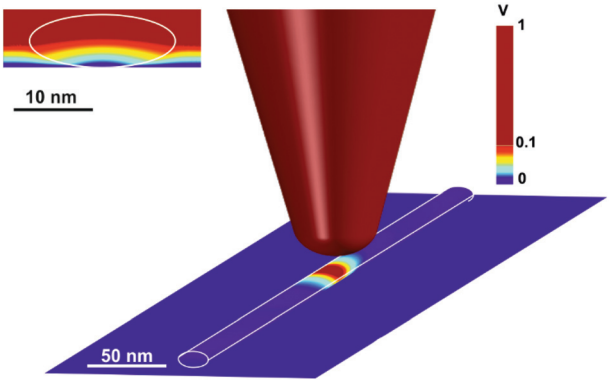

Fig. 1 Example of the electric potential distribution obtained by solving the 3D tip-flagellum electrostatic model by means of finite element numerical calculations. The simulations show that only a narrow portion of the flagellum, containing a few hundreds of flagellin protein monomers, is probed. Parameters used in the numerical calculations: cone height H = 12.5 μm, cantilever width W_c = 3000 nm and length L_c = 3000 nm, half cone angle θ = 11.5°, apex radius R = 24 nm, tip–substrate distance z_{CH} = 28 nm, applied voltage V = 1 V, flagellum height h = 8 nm, width w = 18 nm, length l = 1 μm, and relative dielectric constant, ε_r = 4. Inset: electric potential distribution of a cross-section cut of the axial plane of the flagellum.

nosa PAO1. Flagella are long-thin (~10–20 nm diameter) whip like appendages that bacteria use to move towards the nutrients. They are composed of 11 flagellin protein monomers twisting every ~5 nm.[18] To measure the dielectric constant, we used Scanning Dielectric Microscopy (SDM) as introduced in ref. 8 (see the Materials and methods section). Briefly, SDM combines Electrostatic Force Microscopy (EFM) measurements[19,20] and finite element numerical calculations made with realistic geometrical models. Here, given the filamentous nature of the polar flagella we needed to use 3D electrostatic models. The dielectric constant measured in this way corresponds to a region of the flagellum containing a few hundreds of flagellin protein monomers, as illustrated in the example of the calculated electric potential distribution shown in Fig. 1 (see also discussion below).

Fig. 2a shows topographic atomic force microscopy (AFM) images of two *S. oneidensis* MR-1 and one *P. aeruginosa* PAO1 bacterial cells on a Highly Oriented Pyrolithic Graphite (HOPG) substrate, which show the presence of the polar flagella. Fig. 2b and c show zoom-ins around the respective flagella, while Fig. 2d shows the topographic cross-section profiles taken along the dashed lines in Fig. 2b and c. The dimensions of the *S. oneindensis* flagellum obtained from the topographic images after tip deconvolution (see the Materials and methods section and the ESI†) are height h_{So} = 8.8 ± 0.5 nm, width w_{So} = 18 ± 2 nm, and length l_{So} > 1 μm. For the

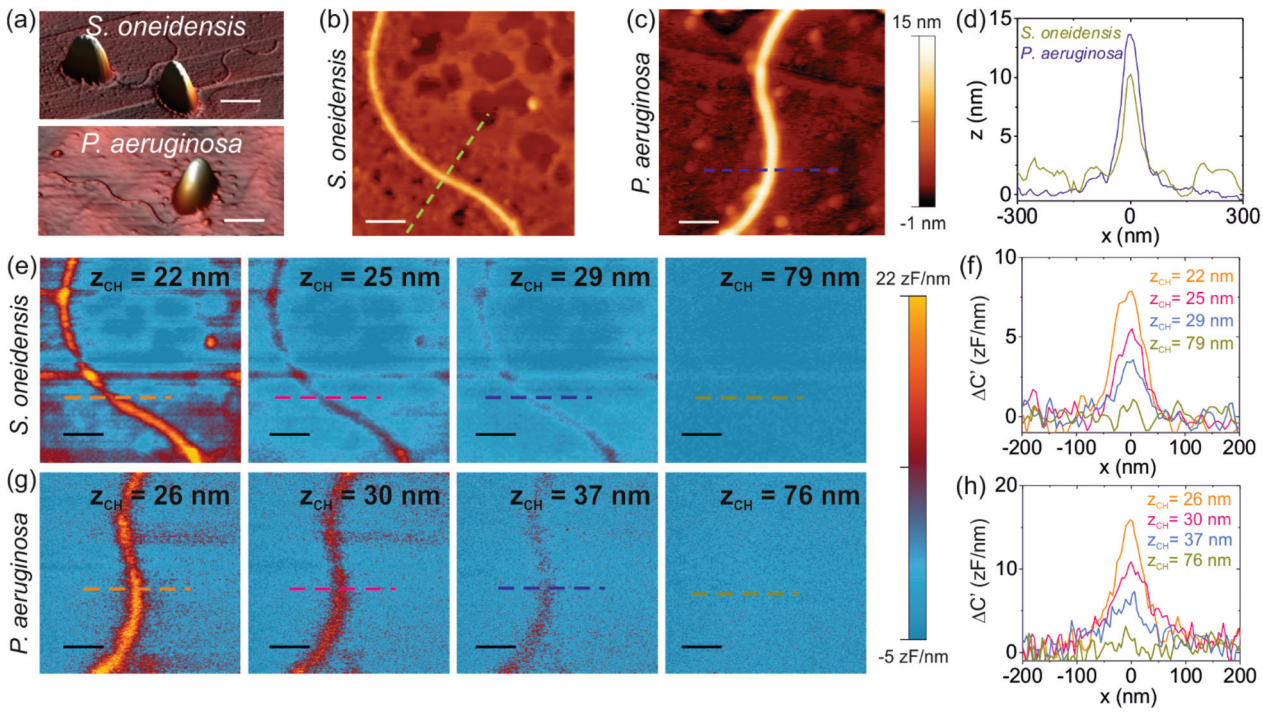

Fig. 2 (a) Topographic AFM images of two *S. oneidensis* MR-1 and one *P. aeruginosa* PAO1 bacterial cells on a HOPG substrate. (b) and (c) Zoom-ins of the images in (a) around the respective flagella. (d) Corresponding topographical cross-section profiles along the dashed lines in (b) and (c). (e) Capacitance gradient EFM contrast images of the *S. oneidensis* MR-1 flagellum at four different tip–substrate distances. (f) Corresponding capacitance gradient cross-section profiles along the dashed lines in (e). (g) and (h) Idem for a flagellum from *P. aeruginosa* PA01. The scale bars in the images in (a) correspond to a length of 1.5 μm and in (b) and (c) to 150 nm. Parameters of the EFM measurements: applied voltage V_{ac} = 3 V and frequency f = 2 kHz, and scan frequency = 1 line per s.

P. aeruginosa flagellum, we obtained h_{Pa} = 12.8 ± 0.5 nm, w_{Pa} = 27 ± 2 nm and l_{Pa} > 1 μm, where the error is the standard deviation over five profiles. The measured flagella dimensions are in good agreement with existing experimental data. For instance, ref. 18 reports a near-atomic resolution cryo-Transmission Electron Microscopy (cryo-TEM) structure of flagellar filaments for different bacteria species, giving for *P. aeruginosa* a radius of ~8.5 nm. With the AFM, we have obtained a half height of ~6.5 nm and a half width of ~13.5 nm, giving an equivalent circular radius of ~9.5 nm, in excellent agreement with the cryo-TEM measurements. This result indicates that the drying and adsorption process only slightly alters the structure of the flagella, producing a slight flattening at a nearly constant area.

Fig. 2e and g show two sets of four constant height EFM capacitance gradient images obtained at distances (z_{CH}) ranging from ~20 nm to ~80 nm for the two types of bacterial flagella considered, respectively. The corresponding capacitance gradient cross-section profiles along the dashed lines in the images are shown in Fig. 2f and h. The dielectric EFM images clearly show the presence of the flagellum especially at the closest tip–substrate distances (<40 nm), with dielectric contrasts up to 10–20 zF nm^{-1} well above the instrumental noise of ~0.7–2 zF nm^{-1}. Note that the dielectric images display regions showing slightly different contrasts. The reason being that the flying tip–substrate distance is set at the ends of each line, and this may slightly change due to the presence of an unavoidable thin layer of residues <1 nm. However, this issue does not constitute any problem for the analysis, which is performed line by line (see the Materials and methods section).

To quantify the dielectric constant of the flagella, we first calibrated the tip geometries, giving a tip radius R_{So} = 23.9 ± 0.5 nm, half cone angle θ_{So} = 11.5° and capacitance gradient offset offset$_{So}$ = 118.5 ± 0.7 zF nm^{-1} for the tip used in the *S. oneidensis* MR-1 flagellum measurements, and R_{Pa} = 30.0 ± 0.5 nm, θ_{Pa} = 11.5°, and offset$_{Pa}$ = 128 ± 2 zF nm^{-1} for the tip used in the *P. aeruginosa* PAO1 measurements (see the Materials and methods section and the ESI†). The tip geometries, together with the deconvoluted flagella geometries reported above, are used to calculate numerically theoretical capacitance gradient images (see the Materials and methods section and the ESI†). Examples of calculated dielectric images at different tip–substrate distances and for different dielectric constants are shown in Fig. 3a and b, respectively, together with the corresponding capacitance gradient cross-section profiles shown in Fig. 3c and d. For numerical efficiency, we used a straight "short" (l = 1 μm) flagellum geometry, instead of the actual long-curved geometry displayed by the flagella (see Fig. 2b and c). This approximation is justified by the locality of the EFM measurements and the moderated curvature of the actual flagella (see the ESI†). Fig. 3e and f show the calculated capacitance gradient maxima as a function of the dielectric constant of the *S. oneidensis* MR-1 and *P. aeruginosa* PAO1 flagella, respectively, at four tip–substrate distances (z_{CH}) (continuous lines). The calculated curves are compared with the experimental measured capacitance gradient values at the center of the flagella (black symbols). The intercept gives the dielectric constant. We obtain dielectric constant values of ε_{So} = 4.3 ± 0.6 and ε_{Pa} = 4.5 ± 0.7 for *S. oneidensis* MR-1 and *P. aeruginosa* PAO1 flagella, respectively, where the error represents, here, the standard deviation of the values obtained at the four tip–substrate distances in each case.

Fig. 3e and f also show the capacitance gradient values measured on the bare HOPG substrate (grey symbols), which are used to set the tip–substrate distances (and hence matching the dielectric constant of unity by definition). The reliability of the extracted dielectric constant values has been further confirmed by comparing experimental capacitance gradient approach curves recorded on top of the flagella with theoretically calculated ones, and by comparing the full experimental capacitance gradient EFM profiles with the calculated ones (see the ESI†). Remarkably, after considering the respective tip and sample geometries, the dielectric constant values obtained for the two types of flagella are almost the same.

The same procedure described above was repeated for three different additional flagella of *S. oneidensis*, obtaining in all cases similar values for the extracted dielectric constant (see Fig. 3g). The overall ensemble average value for the relative dielectric constant (N = 4) is ε_{So} = 4.1 ± 0.4 (see the ESI† for additional data).

Determining the dielectric constant of proteins is an inherently complex problem, due to their microscopic nature and to their unavoidable interaction with the solvent or environment (*e.g.* solution electrolytes or the cell membrane). In fact, measurements performed on protein solutions (*e.g.* by impedance spectroscopy) reflect both the dielectric properties of the proteins, as well as those of the protein–solvent interface[21] and interfacial water molecules.[22] On the other side, measurements performed on dry crystal powders reflect only partially the structure and dynamics of proteins under native conditions.[6] Scanning dielectric microscopy enables measuring the dielectric constant under dry conditions, to get rid of solution effects, and on natural protein macromolecular complexes.

In this work, we measured the dielectric constant of the filamentous part of polar flagella, composed of flagellin proteins,[23] of two distinct types of bacteria, namely *S. oneidensis* MR-1 and *P. aeruginosa* PAO1. The obtained dielectric constants fall within a relatively short range of values ε_r ~ 4–4.5, well defined by the small uncertainty of the measurements (less than ~15%, despite the complexity of the measurements and the small size of the flagella). We note that while the amino acid sequences of the terminal regions of flagellin, including about 180 NH_2-terminal and 100 COOH-terminal residues, are known to be well conserved from species to species of bacteria, the central region can be highly variable.[24] In the case of *P. aeruginosa* flagellin protein (FliC) is 122 amino acids longer in the central region of the protein compared to the *S. oneidensis* flagellin. Despite that, the dielectric response of flagella from *P. aeruginosa* PAO1 and *S. oneidensis* MR-1 was very similar.

Furthermore, the dielectric constant found for the flagella is similar to the values obtained by means of the same tech-

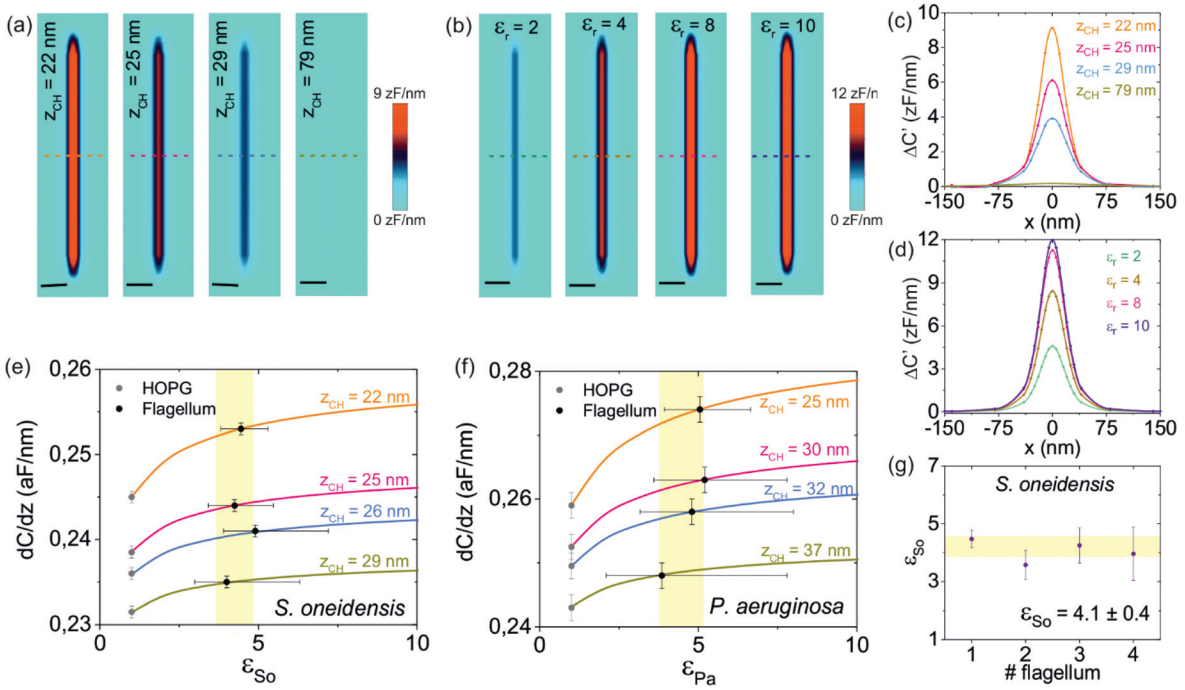

Fig. 3 (a) Examples of calculated capacitance gradient contrast EFM images at four different distances z_{CH} = 22, 25, 29 and 79 nm of a straight flagellum with given dielectric constant ε_r = 4.3. The tip and flagellum geometry correspond to the ones used to quantify the *S. oneidensis* MR-1 flagellum (see below). (b) Idem but for a given tip substrate distance z_{CH} = 22 nm and four different dielectric constants of the flagellum, ε_r = 2, 4, 8, and 10. (c) and (d) Corresponding capacitance gradient cross-section profiles along the dashed lines shown in (a) and (b). (e) Calculated capacitance gradient profile maxima as a function of the dielectric constant of the *S. oneidensis* MR-1 flagellum for four tip–substrate distances (continuous lines). An offset equal to offset_{So} obtained during the tip radius calibration and representing the cantilever effects (not simulated) has been added to the calculated values. The black and grey symbols represent, respectively, the experimental capacitance gradient values obtained from the EFM images in Fig. 2 at the center of the flagellum and on a bare part of the substrate. The latter ones are used to set the tip sample distance and hence they are set to ε_r = 1. The average dielectric constant value is ε_{So} = 4.3 ± 0.6 (shadowed area). (f) Idem for the case of the *P. aeruginosa* PA01 flagellum, giving ε_{Pa} = 4.5 ± 0.7 (shadowed area). (g) Dielectric constant values measured on four different *S. oneidensis* flagella. The overall average dielectric constant value is ε_{So} = 4.1 ± 0.4 (shadowed area). Parameters used in the *S. oneidensis* calculations: R_{So} = 23.9 nm, θ_{So} = 11.5°, h_{So} = 8.4 nm, w_{So} = 18 nm and l_{So} = 1000 nm, offset_{So} = 118.5 zF nm^{-1}. Parameters used in the *P. aeruginosa* calculations: R_{Pa} = 30.0 nm, θ_{Pa} = 11.5°, h_{Pa} = 13.0 nm, w_{Pa} = 27 nm and l_{Pa} = 1000 nm, offset_{Pa} = 128.5 zF nm^{-1}. For the specific parameters used in (g), see the ESI.†

nique in other macromolecular protein complexes, such as the T7 bacteriophage virus capsid (ε_r = 3.5 ± 0.5)[8] and virus tail (ε_r = 3.4 ± 0.4),[9] or submicrometric monolayer patches of bacteriorhodopsin (ε_r = 3.3 ± 0.3).[10] However, they differ from those obtained on macromolecular complexes of other cellular components, such as micrometric lipid bilayer patches (DOPC, ε_r = 1.9 ± 0.3), cholesterol crystals (ε_r = 2.1 ± 0.3),[10] T7 bacteriophage full viruses (ε_r = 6.3 ± 0.4)[8] and T7 bacteriophage DNA (ε_r = 8.5 ± 1.4).[9] The present results thus support the use of dielectric constant values in the range $\varepsilon_r \sim$ 3–4 for the hydrophobic part of proteins, which is believed to account for electronic polarization and small backbone fluctuations.[4] Whether there is a functional reason for the dielectric constant of proteins to take values in the intermediate range between that of lipids and DNA, or whether there are some proteins showing markedly different dielectric behaviour, still needs to be further investigated.

The SDM dielectric measurements reported here are local and at the nanoscale. The dielectric constant obtained for the flagella reflects the dielectric constant of a very small portion of the flagella. The length of this portion, referred to as the dielectric probed length, can be determined as the length of the flagellum starting from which the dielectric contrast reaches a value independent of the length of the flagellum (see the ESI†). Fig. 4 (black symbols, left axis) shows the dependence of the dielectric probed length as a function of the tip radius for the case of the *S. oneidensis* flagellum. For the tip radius used in the present study (~25 nm), the probed length of the flagella is ~130 nm, which corresponds to ~250 flagellin protein monomers,[17] which is a remarkably small number.

Improving the locality of the dielectric measurement on full flagella structures, and hence probing a smaller number of protein monomers, is barely possible by using the presented approach, since further reducing the tip radius and/or the cone angle only moderately improves the locality of the dielectric measurement (see the tendency of the dielectric probed length in Fig. 4 for the smallest radii). Moving to force gradient detection could improve somehow the locality of the measurement (the dielectric probed length in this case reduces by a factor of 0.5–0.7, see the ESI†), but still the number of proteins

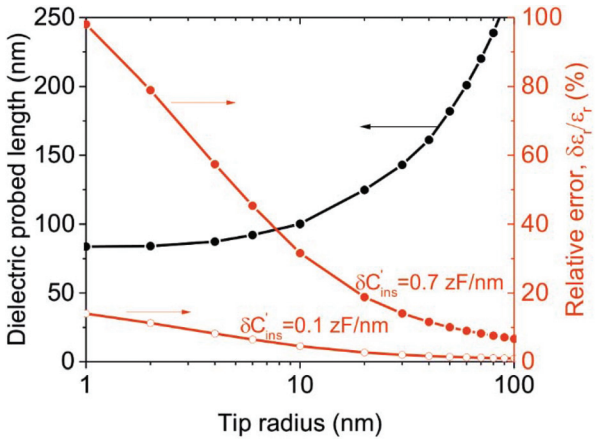

Fig. 4 (Left axis, black symbols) Numerical calculated length of the flagellum probed dielectrically by means of the SDM measurements as a function of the tip radius. (Right axis, red symbols) Relative error in the extracted relative dielectric constant as a function of the tip radius for two different instrumental noise levels $\delta C'_{inst}$ = 0.7 zF nm^{-1} (filled red symbols) and 0.1 zF nm^{-1} (empty red symbols). Lines are guides to the eyes. Parameters used in the calculations: R = 23.9 nm, θ = 11.5°, h = 8.4 nm, w = 18 nm, l = 1000 nm, ε_r = 4.1 and z_{CH} = 22 nm.

probed is relatively large. Probing a significantly smaller number of flagellin protein monomers using this technique would require considering flagella portions (instead of full flagella), with a length shorter than the dielectric probed length discussed above. Under these conditions and based on previous studies,[10] it should be possible to attain the few flagellin monomer limit.

Reducing the tip radius or the length of the flagella would increase the uncertainty of the dielectric constant due to a reduction of the signal to noise ratio. We show it in Fig. 4 (red symbols, right axis) where we plot the relative error in the dielectric constant extraction as a function of the tip radius for the instrumental noise level of the present work, $\delta C'_{inst}$ = 0.7 zF nm^{-1} and for the state of the art noise level, $\delta C'_{inst}$ = 0.1 zF nm^{-1}.[8] The relative error has been calculated according to the relationship

$$\frac{\delta\varepsilon_r}{\varepsilon_r} = \frac{\delta C'_{inst}}{\varepsilon_r \frac{\partial}{\partial \varepsilon_r}\Delta C'(z, \varepsilon_r, R)} \quad (1)$$

where $\Delta C'(z, \varepsilon, R)$ is the maximum contrast for a given tip–substrate distance, z, relative dielectric constant of the flagellum, ε_r, and tip radius, R (see the ESI†). For the tip radii used in the present work (~25 nm) the relative error in a single measurement is ~15%, which can be reduced below a ~10% by averaging several measurements. However, for smaller tip radii (~5 nm), or for short portions of flagella, the error in the extraction of the dielectric constant would quickly rise to unacceptable values (>30%), unless the instrumental noise is decreased down to at least ~0.1 zF nm^{-1} (empty red symbols in Fig. 4).

On wet samples, the overall dielectric response of proteins might slightly increase due to contributions coming from polar end groups and from eventual tightly adsorbed water molecules. The contribution of the hydrophobic core of the protein, instead, is expected not to be significantly affected. For this respect, we note that recent findings on the very low dielectric constant of confined water[22] might give rise to a smaller increase in the dielectric response of the shell region than expected.

Finally, we remark that the present approach should be applicable to most filamentous protein nanostructures present in cells, such as actin or myosin filaments, microtubules or intermediate filaments, including protein nanofilaments relevant for some diseases, such as amyloid fibers,[17] thus spanning significantly the number of proteins accessible to dielectric quantification.

Materials and methods

Scanning dielectric microscopy

We obtained dielectric images by using EFM[19,20] in the amplitude detection mode at constant height, as described in ref. 8. Data are reported in terms of the capacitance gradient, which is related to the electrostatic force at the 2ω harmonic, $F_{2\omega}$, by $C'(z) = 4\ F_{2\omega}\ (z)/V_{ac}{}^2$, where V_{ac} is the amplitude of the ac applied voltage. Capacitance gradient approach curves were recorded on the substrate to determine the tip–substrate distance at which each line has been acquired, and, to calibrate the tip geometry, following the tip calibration procedure explained elsewhere[8] (see also the ESI†).

Measurements were performed with a commercial AFM,[25] Cypher S from Asylum Research, using its internal lock-in to apply the ac voltage and to read the amplitude and phase of the electrostatic probe oscillation. Measurements were performed under controlled dry air conditions (RH < 1%) maintained by a N_2 flow. We used platinum silicide conductive probes (PtSi-CONT, Nanosensors) with a spring constant k ~0.2 N m^{-1} (determined by the provider according to the probe dimensions), resonance frequency f_r ~ 13 kHz, nominal radius R ~ 20 nm and half cone angle θ ~ 11.5°. The analysis of the data was carried out using the WSxM software[26] (Nanotec Electrónica S.L.) and custom-made software developed in Matlab (The Mathworks, Inc.). Dielectric images were obtained in the SNAP mode of the Cypher S (the built-in line by line constant height mode). All EFM data were obtained with a voltage amplitude V_{ac} = 3 V at frequency f = 2 kHz (well below the mechanical resonance peak). The capacitance gradient instrumental noise was in the range ~0.7–2 zF nm^{-1} depending on the probe used and recording parameters.

Finite-element numerical calculations

We used finite element numerical calculations to simulate theoretical EFM capacitance gradient images and approach curves. These data were used in the quantitative analysis of the experimental EFM measurements. The tip was represented like in previous studies[27,28] as a truncated cone of half-angle θ and cone height H terminating in a tangent hemisphere of radius

R. A disc of thickness W_c and with a radius that oversees the cone base by an amount L_c is located onto the cone base, and it models local cantilever effects. Nonlocal cantilever contributions have been considered through a phenomenological capacitance gradient offset contribution term. We used a single angle cone model, as in ref. 8, instead of a two-angle cone model that would better reflect the real geometry of the PtSi-CONT tips, since measurements are restricted to very short distances (<70 nm). In this distance range, single and double cone angle models provide almost identical results,[28] while single angle models largely facilitate its 3D modelling.

The flagellum is modeled as a straight elliptic cylinder with axes w and h for the base ellipse, and length l. The flagellum is assumed to lie on a metallic substrate. Non-straight flagella geometries (*e.g.*, curved elliptic cylinder) have also been considered, producing negligible differences with respect to a straight elliptic cylinder for the actual experimental geometries (see the ESI†). The straight geometry has been kept for computational efficiency. A schematic three-dimensional representation of the tip-flagellum model used for the numerical calculations is shown in the ESI.†

The capacitance gradient between the tip and the sample was calculated by solving Poisson's equation with the AC/DC electrostatic module of Comsol Multiphysics 5.3. We set the surface of the tip to "terminal", the bottom boundary of the simulation domain to "ground", and the top and side boundaries to "zero charge". The infinite element function is used on the top and side boundaries to get rid of finite size effects of the simulation domain. We calculated the electric force on the tip by integration of the Maxwell stress tensor on the tip surface (see further details in ref. 8). The simulation domain was cylindrical with radius ~16 μm–25 μm and a height ~30 μm–50 μm, depending on the tip position with respect to the filament. The mesh was set to a minimum of 6×10^5 elements (see the ESI†). An accurate process of optimization, validation, and numerical noise reduction of the 3D simulations has been performed, to meet sub-0.1 zF nm^{-1} noise accuracy (see the ESI†).

Automatic software routines written in Matlab (The MathWorks, Inc.) have been used to compute capacitance gradient images. In the calculations, the tip moves at a constant height with respect to the substrate. In addition, capacitance gradient approach curves have been also recorded by varying the tip–substrate distance.

Probe geometry calibration

The tip geometry has been determined as in ref. 8 by fitting a short range (15–60 nm) capacitance gradient approach curve recorded over a bare part of the metallic substrate with calculated theoretical capacitance gradient approach curves, with the tip radius and capacitance gradient offset as free parameters. The remaining tip parameters were set to their nominal values: θ = 11.5° H = 12.5 μm, L_c = 3 μm and W_c = 3 μm. As we mentioned above, the use of a single cone angle model tip is justified for the sharpened tips used in the present work because only short-range distances are considered in the EFM approach curves used for the tip calibration and in the image acquisition.[29]

Flagellum width deconvolution

The flagella width, w, was obtained by fitting the measured topographic profile with the analytical spherical tip-ellipse convolution expression,

$$Z_{conv}(X) = \left(\frac{h}{2} - \frac{w^2}{2h}\right)\sin(\alpha(X)) + X\frac{w}{h}\tan(\alpha(X)) - R + \frac{h}{2} \quad (2)$$

$$X = \frac{w}{2}\cos(\alpha(X)) + \frac{R}{\sqrt{1 + \left(\frac{w}{h}\tan(\alpha(X))\right)^2}} \quad (3)$$

where h is the measured flagella height and R is the calibrated tip radius. Eqn (2) and (3) can be used to calculate the tip convoluted profiles if the tangent point between the tip apex and the ellipse is at a height smaller than $R(1 - \sin(\theta))$, which was the case for the tips used in the present work. For smaller tip radii, one must introduce also the contribution of the tip cone in the calculation of the tip convolution. A written Matlab (The MathWorks, Inc.) code was written to implement this procedure automatically. Further details are given in the ESI.†

Dielectric constant extraction

The relative dielectric constant of the flagella ε_{flag} was determined as in ref. 8 from the experimental capacitance gradient images obtained at different tip–substrate distances, by considering the values of the capacitance gradient contrast at the center of the flagella (maximum). These experimental capacitance gradient values were compared with simulated capacitance gradient curves as a function of the flagellum dielectric constant numerically obtained by using the deconvoluted flagellum geometry and the calibrated tip geometry at the given experimental tip sample distance. The extracted values for ε_{flag} from a given image correspond to the mean and standard deviation of the extracted values for the different tip–substrate distances.

Bacteria growth and sample preparation

We used *Shewanella oneidensis* MR-1 (ATCC 700550) cultivated first overnight at 30 °C in Luria–Bertani (LB) (Scharlab) broth under aerobic conditions, and then in minimal AB medium[30] supplemented with 100 mM fumarate and 20 mM lactate during two days under anaerobic conditions at 30 °C in Hungate tubes. We also used *Pseudomonas aeruginosa* PAO1 (ATCC 15692) grown overnight in LB medium at 37 °C under aerobic conditions. The samples for EFM inspection are prepared by taking a drop of the culture solutions, depositing it on a freshly cleaved HOPG and leaving it to rest for 10 min. Afterwards, the drop sample is rinsed two times, first with PBS and second with mili-Q water to remove any poorly adhered cells or any residual from the sample. Finally, we left the sample to dry under ambient conditions. The HOPG substrate was attached to a 1.5 cm diameter magnet using a carbon

double side stick, which was connected to the electrical ground of the atomic force microscope by a small wire.

Conclusions

We have used scanning dielectric microscopy to locally measure the dielectric constant of the filamentous part of bacterial polar flagella composed of flagellin proteins. We have obtained dielectric constant values $\varepsilon_{So} = 4.3 \pm 0.6$ and $\varepsilon_{Pa} = 4.5 \pm 0.7$, for flagella belonging to two distinct types of bacteria, namely, *S. oneidensis* MR-1 and *P. aeruginosa* PAO1, respectively. These values do not depend on the bacterial species and reflect the response of only a few hundred proteins. Similar relative dielectric constant values have been reported for other macromolecular protein complexes using the same technique. Altogether, these results indicate that the relative dielectric constant of proteins under dry conditions show dielectric constant values (~3–5), like those reported using macroscopic techniques applied to dry protein crystals, and different from the values reported for other cell components such as lipids (~2) or DNA (~8). These results may have important implications in the understanding of the relevance of the electrostatic energy contribution to the protein function and structure.

Conflicts of interest

There are no conflicts to declare.

Acknowledgements

This work has been partially supported by the Spanish Agencia Estatal de Investigación and EU FEDER through grants TEC2015-72751-EXP, TEC2016-79156-P and BIO2015-63557-P. G. G. acknowledges support from an ICREA Academia award from the Generalitat de Catalunya and H. L. for an FPI grant (BES-2015-074799) from the Agencia Estatal de Investigación/Fondo Social Europeo. We also acknowledge support from Generalitat de Catalunya (2017 SGR1079 and CERCA Program).

References

1 B. Honig and A. Nicholls, *Science*, 1995, **268**, 1144.
2 K. A. Sharp and B. Honig, *Annu. Rev. Biophys. Biophys. Chem.*, 1990, **19**, 301.
3 M. K. Gilson and B. H. Honig, *Biopolymers*, 1986, **25**, 2097.
4 T. Simonson and C. L. Brooks, *J. Am. Chem. Soc.*, 1996, **118**, 8452.
5 C. N. Schutz and A. Warshel, *Proteins*, 2001, **44**, 400.
6 T. Simonson, *Rep. Prog. Phys.*, 2003, **66**, 737.
7 M. F. Perutz, *Science*, 1978, **201**, 1187.
8 L. Fumagalli, D. Esteban-Ferrer, A. Cuervo, J. L. Carrascosa and G. Gomila, *Nat. Mater.*, 2012, **11**, 808.
9 A. Cuervo, P. D. Dans, J. L. Carrascosa, M. Orozco, G. Gomila and L. Fumagalli, *Proc. Natl. Acad. Sci. U. S. A.*, 2014, **111**, E3624.
10 A. Dols-Perez, G. Gramse, A. Calo, G. Gomila and L. Fumagalli, *Nanoscale*, 2015, **7**, 18327.
11 S. T. Bayley, *Trans. Faraday Soc.*, 1951, **49**, 509.
12 S. Takashima and H. P. Schwan, *J. Phys. Chem.*, 1965, **69**, 4176.
13 M. Bockrath, N. Markovic, A. Shepard, M. Tinkham, L. Gurevich and L. P. Kouwenhoven, *Nano Lett.*, 2002, **2**, 187.
14 W. Lu, D. Wang and L. Chen, *Nano Lett.*, 2007, **7**, 2729.
15 W. Lu, Y. Xiong, A. Hassanien, W. Zhao, Mi. Zheng and L. Chen, *Nano Lett.*, 2009, **9**, 1668.
16 Y. Yang, W. Guo, X. Wang, Z. Wang, J. Qi and Y. Zhang, *Nano Lett.*, 2012, **12**, 1919.
17 T. P. J. Knowles, M. Vendruscolo and Ch. M. Dobson, *Nat. Rev. Mol. Cell Biol.*, 2014, **15**, 384.
18 F. Wang, A. M. Burrage, S. Postel, R. E. Clark, A. Orlova, E. J. Sundberg, D. B. Kearns and E. H. Egelman, *Nat. Commun.*, 2017, **8**, 960.
19 Y. Martin, D. W. Abraham and H. K. Wickramasinghe, *Appl. Phys. Lett.*, 1988, **52**, 1103–1105.
20 P. Girard, *Nanotechnology*, 2001, **12**, 485–490.
21 R. Pethig, *Annu. Rev. Phys. Chem.*, 1992, **43**, 177.
22 L. Fumagalli, A. Esfandiar, R. Fabregas, S. Hu, P. Ares, A. Janardanan, Q. Yang, B. Radha, T. Taniguchi, K. Watanabe, G. Gomila, K. S. Novoselov and A. Geim, *Science*, 2018, **360**, 1339.
23 T. Fujii, T. Kato, K. D. Hiraoka, T. Miyata, T. Minamino, F. F. V. Chevance, K. T. Hughes and K. Namba, *Nat. Commun.*, 2017, **8**, 14276.
24 D. R. Wilson and T. J. Beveridge, *Can. J. Microbiol.*, 1994, **39**, 67.
25 P. Eaton and P. West, *Atomic Force Microscopy*, Oxford University Press, Oxford, 2010.
26 I. Horcas, R. Fernandez, J. M. Gomez-Rodriguez, J. Colchero and J. Gomez-Herrero, *Rev. Sci. Instrum.*, 2007, **78**, 013705.
27 M. C. Biagi, R. Fabregas, G. Gramse, M. Van Der Hofstadt, A. Juarez, F. Kienberger, L. Fumagalli and G. Gomila, *ACS Nano*, 2016, **10**, 280.
28 M. Van Der Hofstadt, R. Fabregas, R. Millan-Solsona, A. Juarez, L. Fumagalli and G. Gomila, *ACS Nano*, 2016, **10**, 11327.
29 L. Fumagalli, M. A. Edwards and G. Gomila, *Nanotechnology*, 2014, **25**, 495701.
30 N. Uría, X. Muñoz Berbel, O. Sánchez, F. X. Muñoz and J. Mas, *Environ. Sci. Technol.*, 2011, **45**, 10250.